(Online) ISSN 2712-0554
Original Research

Heritage and Sustainable Development
Vol. 7, No. 2, 2025, pp.1183-1198
https://doi.org/10.37868/hsd.v7i2.1594

Microstructure and corrosion behavior of Mg-Nd-Fe-B alloys with varying magnet content

Huwaidah Ibrahem Ahmed[1*], Ali Abadi Aljubouri[2], Hanaa A. AL-Kasiy[3]
[1,2] College of Applied Science, University of Technology, Iraq
[3] College of Materials Engineering, University of Technology, Iraq

*Corresponding author E-mail: as.21.26@grad.uotechnology.edu.iq

Received Jun. 1, 2025
Revised Sep. 1, 2025
Accepted Sep. 5, 2025
Online Nov. 12, 2025

Abstract

A systematic study was conducted to evaluate the corrosion behavior of a novel magnesium alloy, Mg–Nd–Fe–B, incorporating varying percentages of neodymium magnet scrap. Immersion tests were performed in a sodium chloride (NaCl) solution at room temperature to assess corrosion resistance. The objective was to enhance the corrosion resistance of a new family of lightweight ternary alloys within the Mg–Nd–Fe–B system. X-ray diffraction (XRD) was employed to identify the crystalline phases, while scanning electron microscopy (SEM) was used to examine the microstructure of samples before and after corrosion. The alloys primarily consisted of α-Mg and $Nd_2Fe_{14}B$ phases. Post-corrosion analysis revealed the presence of corrosion products rich in rare earth elements, with the dominant phase being a solid solution of magnesium and neodymium. Corrosion testing showed the formation of a black, neodymium-based surface layer, which acted as a protective barrier. The corrosion rate decreased significantly with increasing magnet scrap content, with the optimal composition (approximately 30 wt%) achieving an 87.3% reduction in corrosion rate compared to alloys with lower magnet content. Additionally, Vickers hardness testing demonstrated a notable improvement in hardness, further supporting the alloy's suitability for engineering applications. These findings highlight the beneficial role of rare earth elements, particularly neodymium, in improving both the corrosion resistance and mechanical properties of magnesium-based alloys.

Keywords: Magnesium, NdFeB, Corrosion, Magnet, Rare earth

1. Introduction

It is well known that magnesium, the lightest of all structural metals in use today, possesses a density in the range of about 1.74 g/cm^3, thereby presenting a strong competitive advantage for applications demanding light weighting, including the aerospace, automotive, and portable electronic devices industries [1]. It also has excellent mechanical characteristics, i.e., vibration damping, shock absorption, and machining. Yet, one of the most important barriers to using magnesium in various industries is its susceptibility to corrosion, especially in

the presence of chloride ions [2], [3].

To overcome these problems, alloys have been developed that are provided with components increasing structural and chemical properties. Rare-earth elements (REE), including neodymium (Nd), are one of the most popular additions for improving corrosion resistance. The introduction of neodymium in magnesium alloys leads to its precipitation in other phases ($Mg_{12}Nd$, $Mg_{41}Nd_5$), supporting the modification of grains and impeding the penetration of the corrosive medium [4], [5].

Recent investigations have found the possibility of neodymium to also generate quite stable corrosion products (e.g., $Nd(OH)_3$), which would be able to reduce the global corrosion rate by restricting the contact of the metal with the oxidizing solution [6], [7]. These stages also contribute to increased structural homogeneity and a reduction in the number of localized corrosion points, also very important in applications demanding high long-term reliability.

Furthermore, particularly iron (Fe) and boron (B) are becoming more and more important alloying additions. While usually regarded as an undesirable element in Mg alloys (due to the formation of galvanic cells that exploit the difference in potential along the grain boundaries and thus accelerate the corrosion rates) [8], [9]. Careful regulation of the concentration of the Fe and combination with B can result in stable Fe2B or Nd2Fe14B phases that change the microstructure and the corrosion behavior [10].

By adding a different magnetic component, the Fe-B compound, to the Mg-Nd-Fe-B alloy, the microstructure changes greatly. However, it was reported that such an adjustment results in a better size of crystal grains, a solid solution of component metal, and a more consistent distribution, which can improve the properties of corrosion resistance properties of the alloy [11], [12]. Zhenzhen Gui et al. studied the corrosion behavior of the as-cast and solution-treated Mg-xGd-1.5Nd-0.5Zn-0.5Zr alloys. The research concluded that the corrosion resistance of the solution-treated Mg-3Gd alloy attained the lowest value (0.973 mm/yr), due to the large quantities of ZnZrx with a flower-like phase distribution, forming a series of galvanic couple groups with the α-Mg [13].

The aim of this research is to develop Mg-Nd-Fe-B alloys for various applications, such as automotive components, electronic devices, and smartphones, as well as to investigate the effect of the content ratio of magnet on the corrosion characteristics of the Mg-Nd-Fe-B alloys. Also, to understand the fundamental aspects of the corrosion behavior of the newly developed Mg-Nd-Fe-B alloys, and most importantly, recycling NdFeB scrap through this method can reduce the overall cost of producing Mg-Nd alloys. Adding magnesium can enhance certain properties of the Nd-Fe-B magnet, potentially leading to better performance in specific applications or environments.

2. Experimental procedure

2.1. Materials

Magnesium powder was obtained from Maclean Company, and neodymium magnets were obtained by collecting a quantity of scrap hard disks, which were dismantled, and the magnets were removed.

2.2. Testing instrumentations

The instruments were: a planetary ball mill, a pressing mold with a diameter of 1 cm and a height of 4 cm, a hydraulic press with a pressure of 10 tons, and a vacuum electric oven, NQM-0.4 Model planetary ball mill (Yangzhou Nuoya Machinery Co., Ltd.), particle size analyzer nano brook (90 Plus), Brookhaven Instruments Corporation Mineral, Manual Hydraulic Press (Han14468), MTI, Tube Furnace GSL 1600X from Lab World Group USA, Potentiostat/Galvanostat Corr test model CS350M, Chi. All of the above are available at the University of Technology, Nanotechnology Advanced Materials Research Centre, Baghdad, Iraq. The Axia Chemi SEM is a product of Thermo Fisher Scientific, a global company. XRD is a product of Malvern Panalytical, a spectroscopy company. The Digital Micro Vickers Hardness Tester TH714.

2.3. Collection and preparation of magnet scrap

After obtaining a set of non-working hard drives, the screws and outer covers were removed. A neodymium magnet is located inside the disk. After obtaining a group of magnets, we remove the outer layer of nickel plating using a scraping process. The demagnetization process was carried out at 300, 350, 400, and 450°C for 15 and 30 minutes, respectively. The magnets are very fragile and thin, and can be broken easily. The scraps were crushed and milled in a lab. A ball mill MTA, USA) at 450 rpm for 60 minutes to produce a fine particle size was then analyzed for the particle size and composition. The amount of nickel and remaining metal content in the magnets is determined by energy dispersive X-ray spectroscopy (EDX).

2.4. Mg-Nd-Fe-B alloy preparation

Magnesium powder was sourced from Maclean Company and was further milled using a planetary ball mill to achieve a fine particle size. Neodymium magnet powder was obtained by collecting several magnets from decommissioned hard disks, crushing them, and grinding them using a planetary ball mill to obtain a powder with a particle size of 64.4 nm. The alloys were incorporated in variable proportions of magnet: 3%, 4%, 10%, 20%, and 30%. The mixture underwent homogenization using a vibrating device. The pressing was done using a mold with a diameter of 1 cm and a height of 4 cm. This mold was placed in a hydraulic press operating at a pressure of 8 tons. Following the extraction of samples, which was presented in Figure 1, the sintering process was conducted using a vacuum electric oven model GSL1600 X from MTI Corporation.

The compressed samples, which contained different percentages of neodymium magnet scrap powder, were placed in small alumina crucibles, and the sintering process was executed at a temperature of 500°C for 1 hour, followed by cooling within the oven. The preparation of samples for examination via scanning electron microscopy involved the use of silicon carbide paper, ranging from grit 400 to 1000. Smoothing began with the course 400 grit paper and utilized water for residue removal, with the sample being rotated 90 degrees at each progression between different grits. Once this was completed, the samples were washed with water, and polishing was carried out using a polishing device equipped with a specialized cloth affixed to a rotating disc, along with polishing paste.

This procedure continued until all smoothing lines were eliminated and the surface achieved a mirror-like finish. Subsequently, the samples were rinsed with water and alcohol, then dried using a drying device. An etching solution was prepared, consisting of 1 mL of HNO_3, 24 mL of water, and 75 mL of ethylene glycol, placed in a watch glass. Each sample was immersed in this solution for 3-5 seconds, removed, and washed with water and alcohol, followed by drying until ready for examination [14],[15].

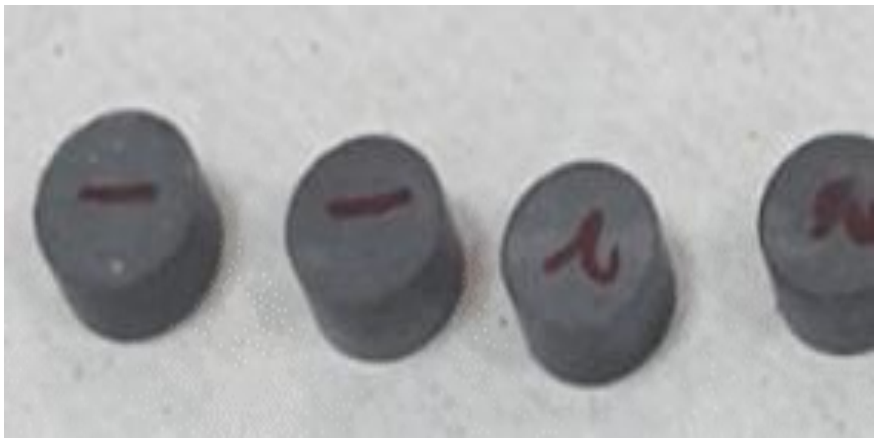

Figure 1. Samples of Mg-Nd-Fe-B alloys

2.4.1. Corrosion testing methods

Potentiostat/Galvanostat Corrosion test model CS350M is used to measure polarization resistance and the corrosion rate. The method of operation is summarized by preparing the three electrodes inside the corrosion

cell, then connecting the three electrodes to the connections of the corrosion device. We press the power button on the device, then turn on the calculator in the device, then click on the CS Studio icon, and finally, the OCP examination process is performed on the sample. A 3.5% sodium chloride saline solution was prepared and placed in the designated place within the apparatus. One-centimeter-diameter and one-centimeter-high cylindrical samples were immersed in the solution for 15 minutes, and the corrosion current and corrosion rate were calculated using the same device.

3. Results and discussions

3.1. Magnet characterization

The milled demagnetized permanent magnet waste was analyzed using EDX. The illustrated samples that were demagnetized predominantly comprise the elements Fe and neodymium, together with small amounts of boron, dysprosium, and praseodymium, as listed in Table 1. The EDX analysis, as shown in Figure 2, shows the presence of particles of irregular shape. These results are in agreement with those reported by [16].

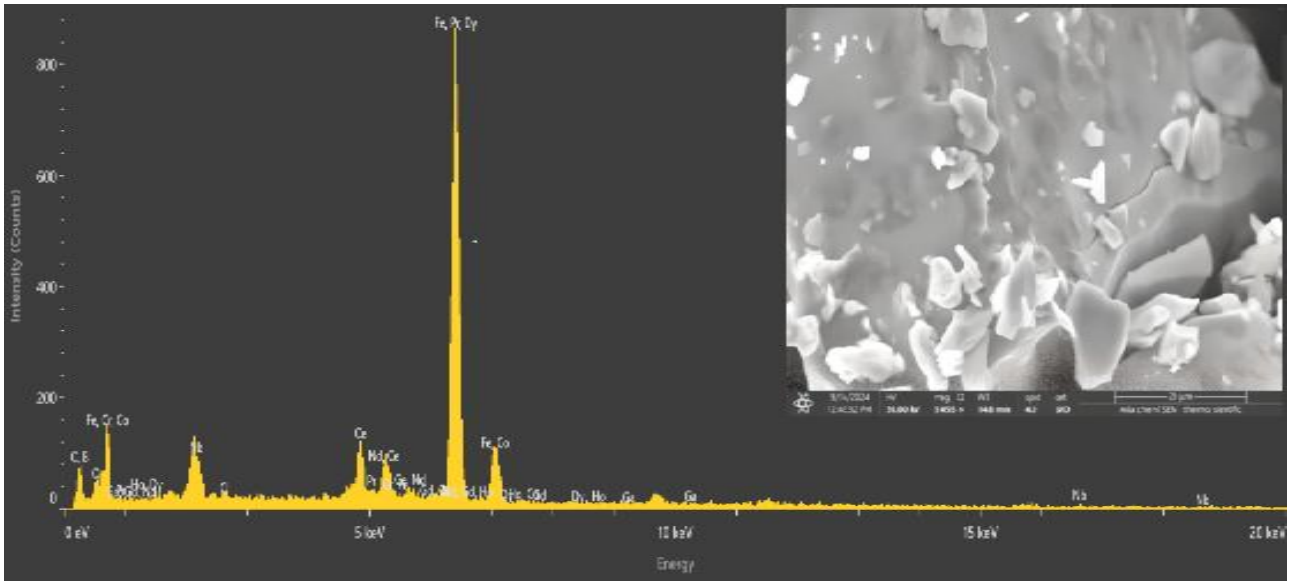

Figure 2. FE-SEM image & EDX analysis of the NdFeB magnet powder

Table 1. Chemical composition of NdFeB magnet waste (EDX analysis)

Element	B	Cr	Fe	Co	Ga	Nb	Ce	Pr	Nd	Gd	Dy	Ho	Ni	Zr
Weight %	1.7	0.1	62.1	0.1	0.2	1.0	1.3	2.2	29	0.05	1	0.6	2.0	0.95

3.2. X-ray diffraction (XRD) analysis for magnet scrap

The X-ray diffraction (XRD) pattern of an NdFeB, as shown in Figure 3, predominantly indicates the presence of the $Nd_2Fe_{14}B$ tetragonal phase, which is the principal magnetic phase responsible for the material's profound magnetic properties. The peak positions, represented by the 2θ values, along with their relative intensities, may be systematically compared with those established by JCPDS #40-1028. In neodymium iron boron magnets, the significant diffraction peaks in the XRD patterns are typically located at the following 2θ values: 24.20°, 33.23°, 35.70°, 40.95°, 49.57°, 54.20°, 62.58°, 64.15°, and 72.14°. These peaks correlate with the 012, 104, 110, 113, 024, 116, 214, 300, and 1010 reflections of the $Nd_2Fe_{14}B$ tetragonal crystalline structure. The study confirms prior findings about [17], [18].

Furthermore, peaks observed at approximately 44.02° and 49.62° are indicative of the $Nd_2Fe_{14}B$ phase. The pattern also reveals peaks corresponding to other minor phases, including Nd-rich phases (for instance, Nd or Nd2O3) [19].

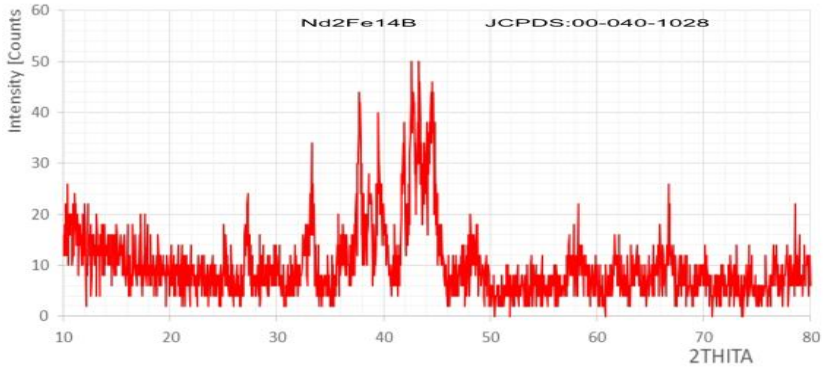

Figure 3. (XRD) Pattern for NdFeB magnet scrap

3.3. Particle size analysis

The particle size of magnet powders plays a significant role in determining the microstructure and, consequently, the physical and magnetic properties of Mg-Nd-Fe-B alloys. While much of the research focuses on Nd-Fe-B systems, the principles extend to Mg-containing variants, particularly regarding sintering, grain growth, and phase distribution. Referring to Figure 4, the grain size is equal to 64.4 nm, which is a very suitable value for alloying with magnesium [20].

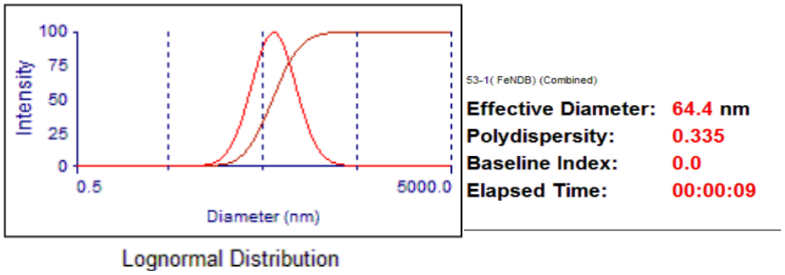

Lognormal Distribution

Figure 4. Particle size of the neodymium magnet scrap

3.4. Corrosion of pure magnesium

Mg has a relatively high corrosion rate in comparison with many structural metals, and pitting corrosion, as shown in Figure 5, is the most problematic type of corrosion in this metal. Pitting corrosion is a very localized and aggressive form of corrosion that can initiate through a passive film or surface covered by a thin corrosion product film. The pit is characterized by its small diameter. When the thickness of a barrier-like protective oxide decreases due to localized removal, local erosion of the base material might occur, leading to the formation of small deep pits in it. Thus, pitting corrosion has to be considered an accelerated form of the first stage of localized attack. Pitting causes damage to the metal surface [21], [22].

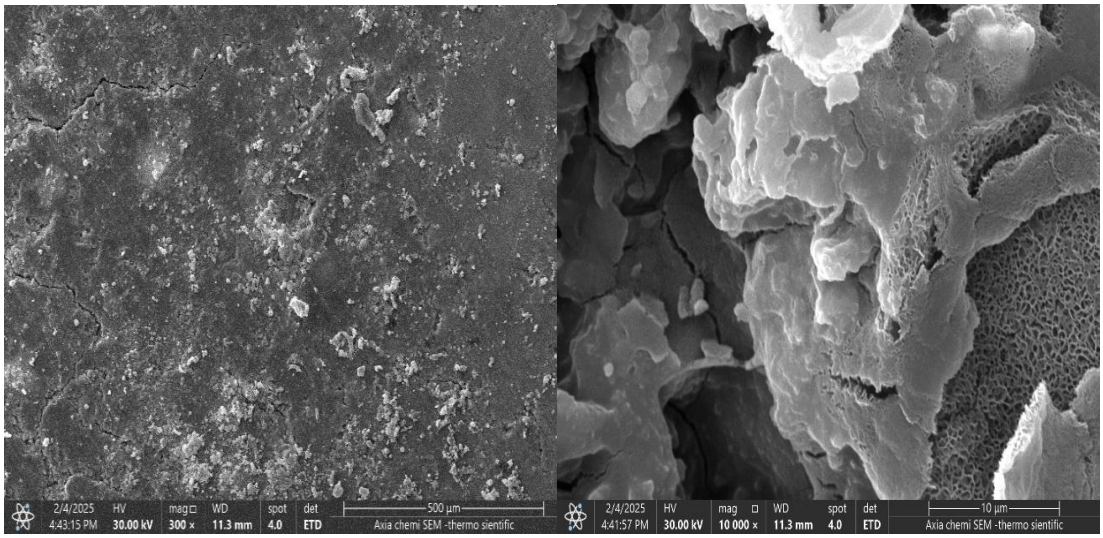

Figure 5. FE-SEM images for the pitting corrosion of pure magnesium at 300x and 10,000x magnification

3.5. Microstructure and phase transformations in Mg-Nd-Fe-B

Microstructures in Mg-Nd-Fe-B alloys are fundamentally a function of the processing. These alloys, as shown in Figure 6, typically contain two main phases: an α-Mg phase with a hexagonal close-packed structure and an $Nd_2Fe_{14}B$ phase with a tetragonal structure occurring in various structures such as grains, grain boundaries, and twins alongside Nd-rich and Fe-rich phases before corrosion. The additional complex microstructure of the precipitates and the voids in the alloys is tailored to improve the properties for a given application. The soft Nd-rich and Fe-rich phases in bulk magnets boost coercive force through intricate phase interactions, refining the magnetic characteristics. Understanding and optimizing these features is essential for enhancing the performance of Mg-Nd-Fe-B alloys across technological contexts. These alloys possess a vast phase regime and can be observed based on the respective phase diagrams [23].

The formation of the phases is dependent on the composition as well as the temperature. Phase diagrams illustrate the temperature window where an individual single, double, or triple phase region can be observed, and based on these phases, the formation of a particular phase can be anticipated. Understanding phase transformations is mainly important because they affect the properties of the material, and during high-temperature operation, it is imperative for the stability and reliability tuning of the materials [24].

As described, the phase diagram is based on the individual compositions of the elements and MgO, but if we need to have some idea, we could consider the binary systems and individual phase understanding. The individual understanding of the phases can be reflected through available presentations, such as solid-solution transformation, peritectic reactions, eutectic reactions, solvus lines, miscibility gaps, and so on, collectively, where a large range of materials can be studied. The magnetic behavior can be enhanced through a distinct phase ratio because particular phase regimes are generally better compared to others, and a large Nd2Fe14B phase is expected to have a minimal amount of α-Mg, along with the alignment of the grains in the predominantly textured Nd2Fe14B. Moreover, these materials can be thermally treated to realize their optimal magnetic performance [25].

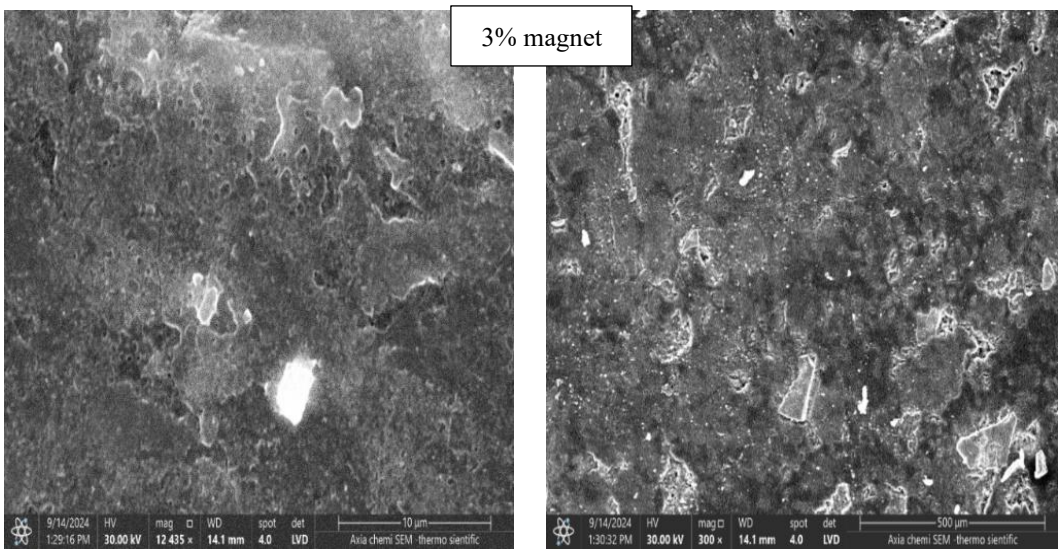

Figure 6a. 3% magnet

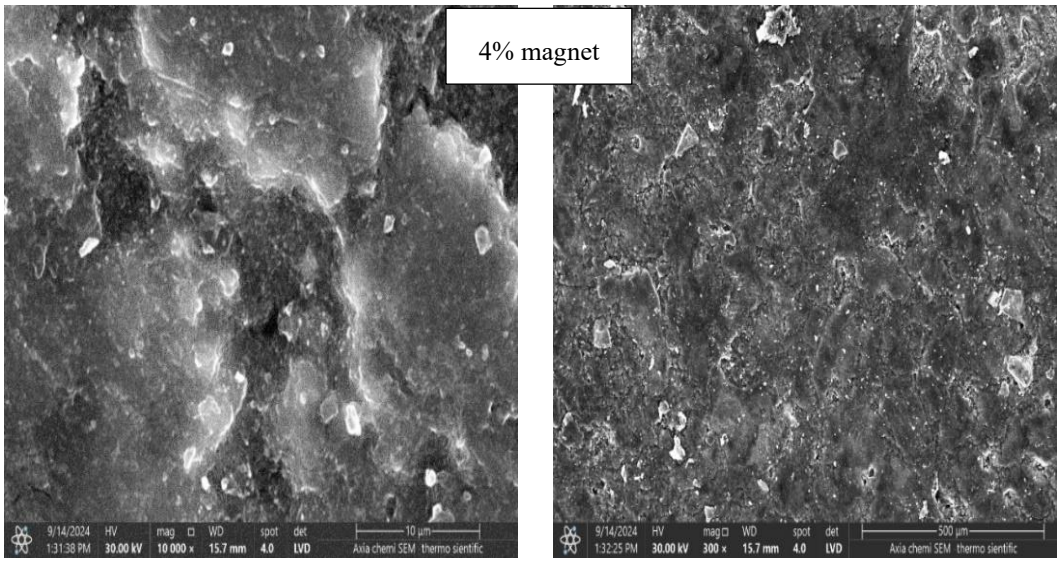

Figure 6b. 4% magnet

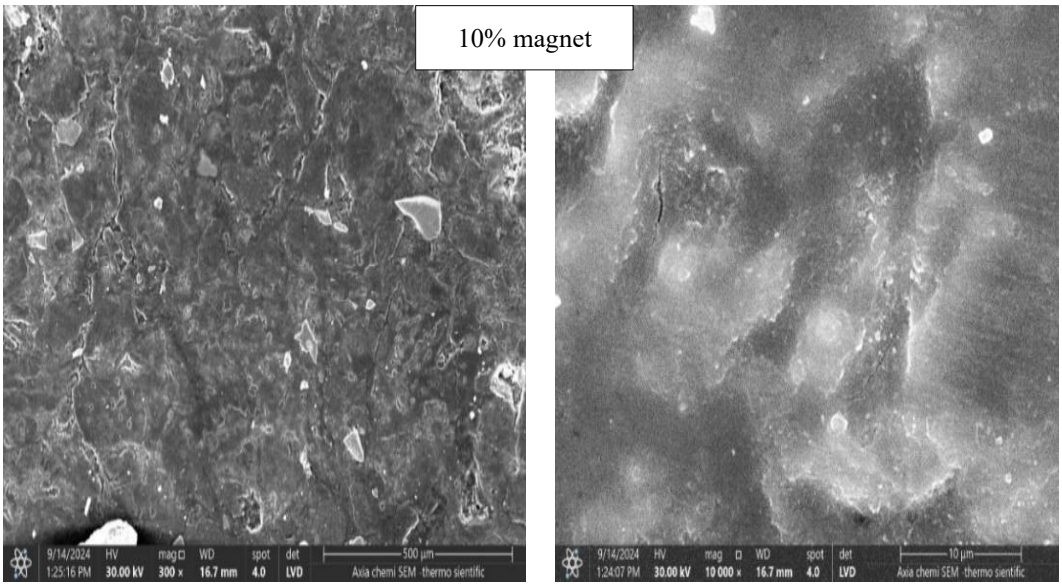

Figure 6c. 10% magnet

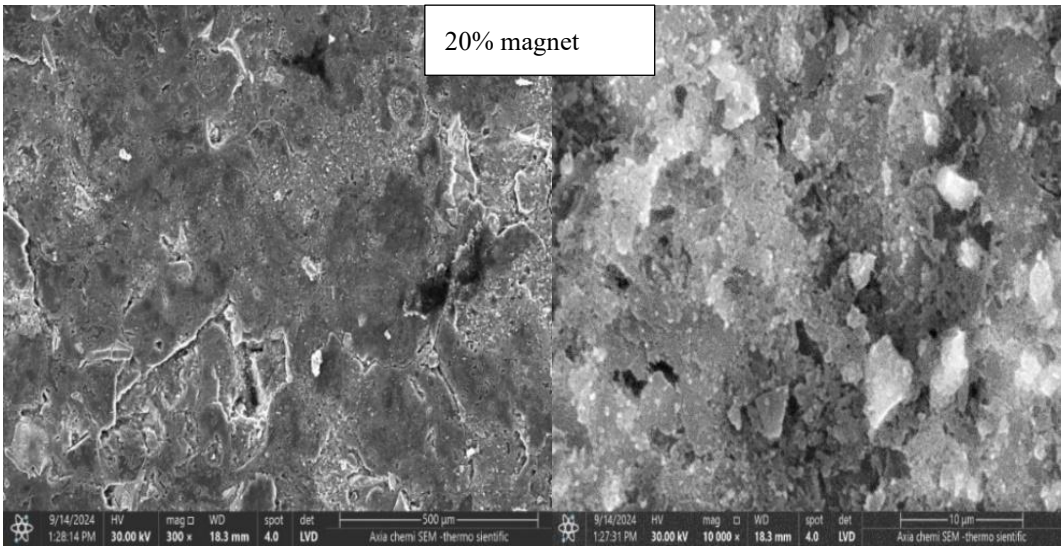

Figure 6d. 20% magnet

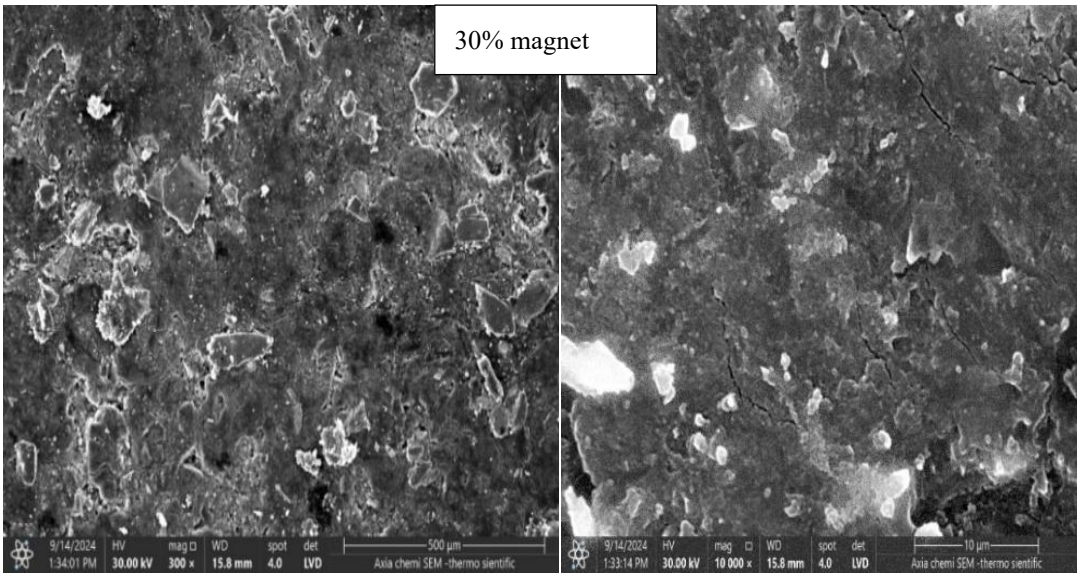

Figure 6e. 30% magnet

Figure 6. Microstructure of Mg-Nd-Fe-B alloys with variable magnet content at 300x and 10,000x magnification for each magnet content

3.5.1. Analysis of Mg-Fe-Nd-B alloy using X-ray diffraction (XRD)

XRD determined the Mg-Fe-Nd-B alloy crystal structure. XRD patterns, as shown in Figure 7, were plotted using diffractometer data. JCCPDS data were used to compare the Nd2Fe14B and α-Mg peaks. The JCPDS card number for $Nd_2Fe_{14}B$ with a tetragonal structure is JCPDS #40-1028 and α-Mg (JCPDS card No. 35-0821), which is a hexagonal close-packed (HCP) structure [26].

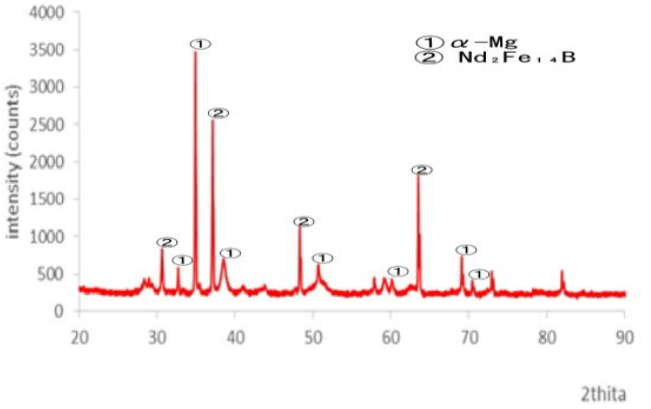

Figure 7. XRD analysis for Mg-Nd-Fe-B alloy at 4% magnet content

3.5.2. Corrosion behavior of Mg-Nd-Fe-B alloys with varying magnet content

After the addition of the rare earth elements Nd and intermetallic phases like Fe_3B, through specific methodical tests and results discussed in this research. The Nd-rich phase was found in the SEM as it forms in the composite of the alloy Mg-Nd-Fe-B boride phase, which is are compound formed by combining neodymium and boron, such as NdB_6, NdB_4, and $Nd2B_5$. These borides are known for their hardness, high melting points, and metallic-like conductivity, making them useful in various applications. On the whole, this phase has been significantly added to the anodic phase, which improves the resistance of the Mg phase, thus stabilizing the Mg alloys. As shown in Figure 8, it can be seen that corrosion products appear as black and white regions on the surface of the magnesium, indicating dense (or compact) and porous corrosion products, and they are uniformly distributed over the entire magnesium surface. This conclusion is in line with recent findings in the field [27].

This means that the entire surface of the tested materials is covered with corrosion products. In addition, the corrosion products deposition on the naked substrates makes the creep effect of the corrosion products impossible. The visibility of corrosion products in “heaps” and not in a layer means that they will not crack or peel off; therefore, the growth of products was seen with visible pores. This study reinforces previous work on the topic [28]. These findings clarify that Nd-Fe-B incorporation into magnesium is the most advantageous compared to the magnesium matrix for corrosion resistivity. The fraction of a second phase in a solid substrate developed during processing has a dramatic effect on corrosion stops. Changes in the fabric of grain boundaries and their junctions with progressively finer grain size, increasing amounts of sub-structuredness, and increased tortuosity have a comparable effect [29], [30]. The increasing concentration of the rare earth by 3, 4, 10, 20, 30% decreases the current of corrosion I_0. The 30% Nd-Fe-B addition ratio has the best corrosion resistance because of its highest pitting potential, low corrosion current density, reasonable compactness, and narrow and deep penetration shape of corrosion products.

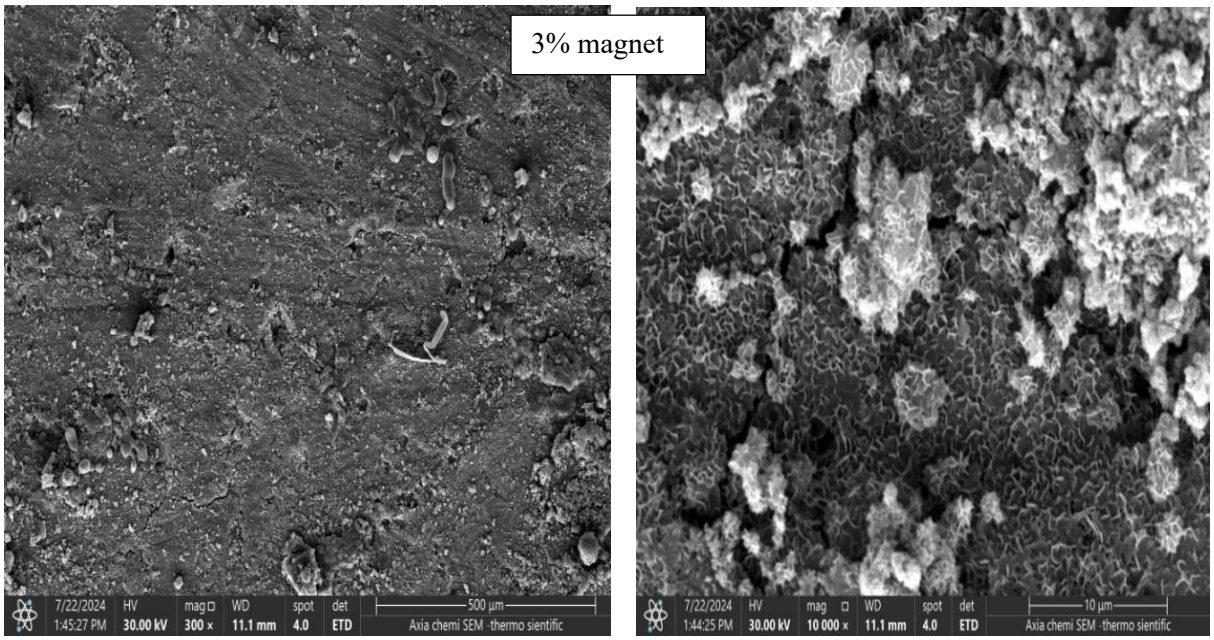

Figure 8a. 3% magnet

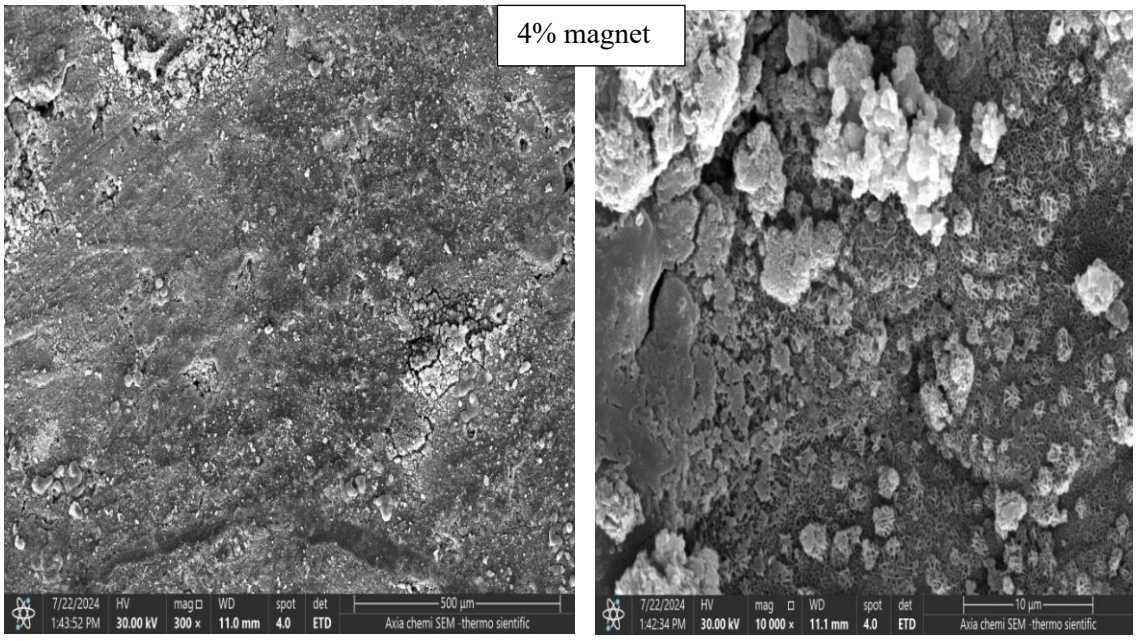

Figure 8b. 4% magnet

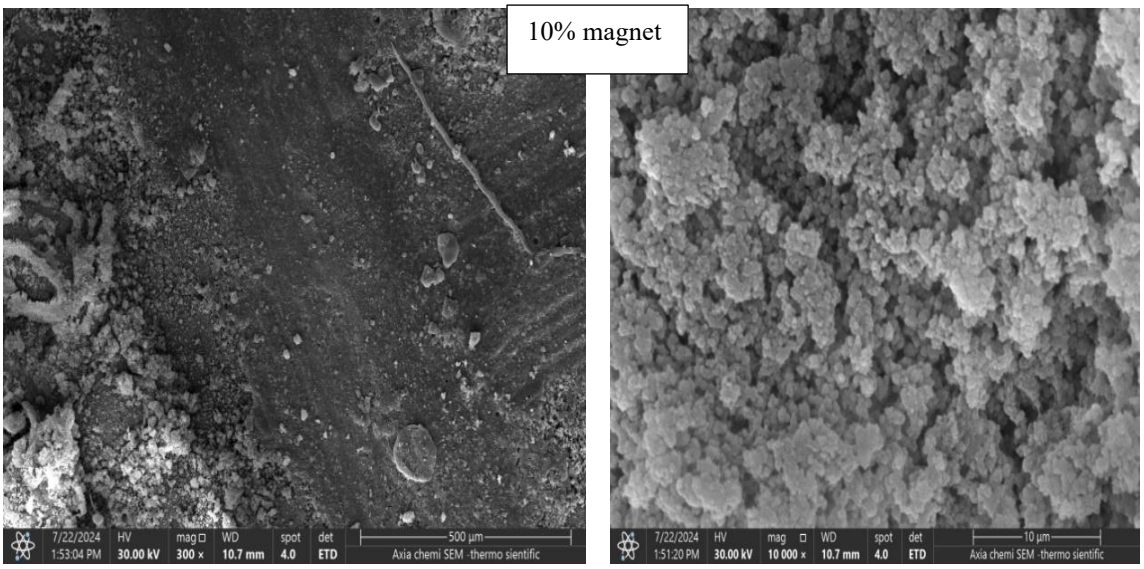

Figure 8c. 10% magnet

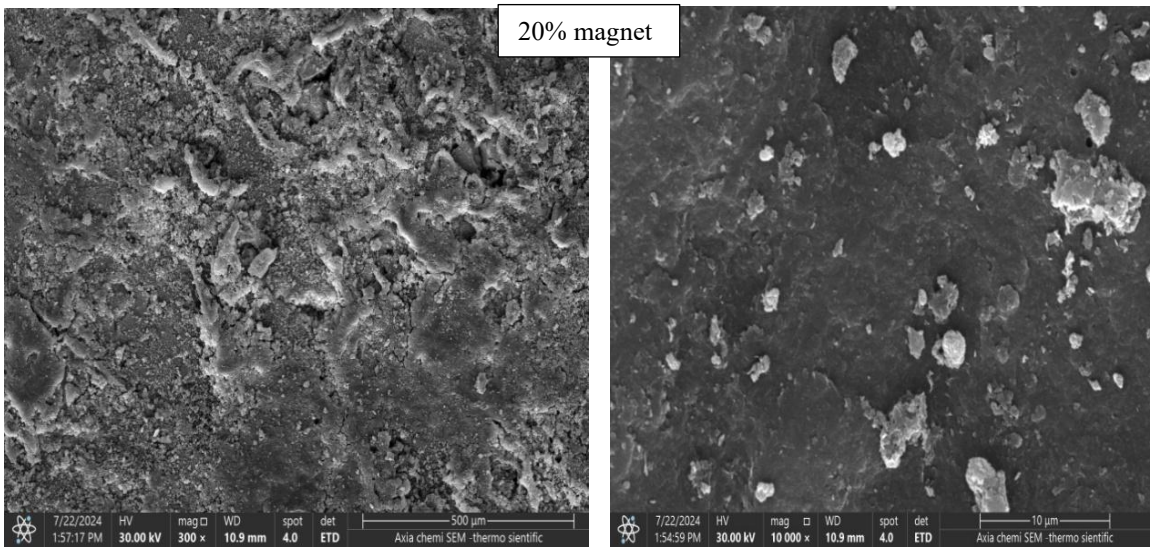

Figure 8d. 20% magnet

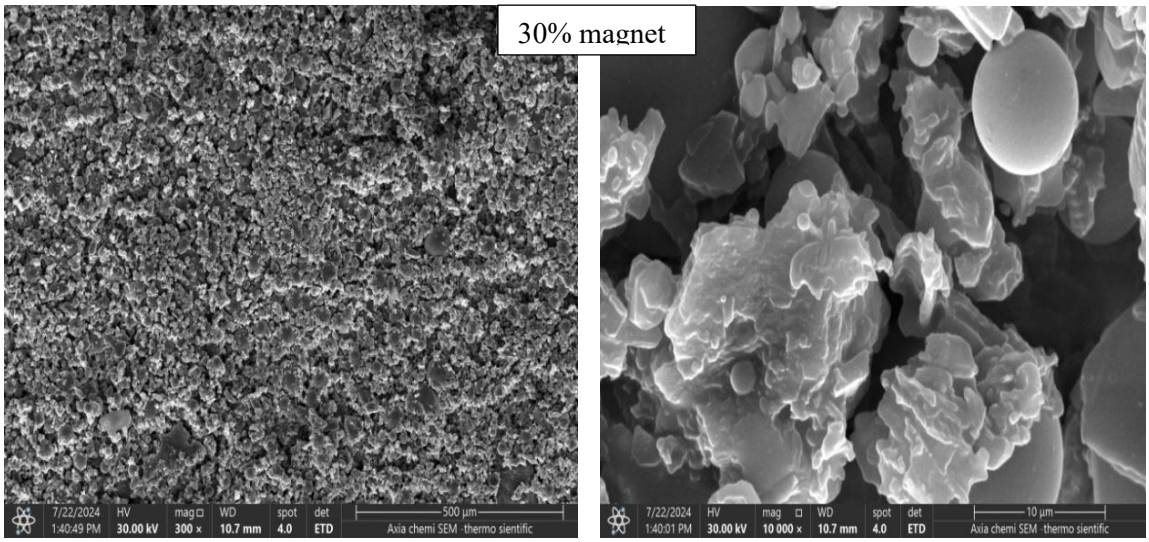

Figure 8e. 30% magnet

Figure 8. Microstructure of Mg-Fe-Nd-B alloy after immersion in 3.5% salt solution with variable magnet content at 300x and 10,000x magnification for each magnet content

3.5.3. Polarization resistance (Rp)

The polarization resistance, Rp, of an electrode is specifically defined as the slope of the potential (E) versus the current density ($i_{\circ}$) around the corrosion potential (Ecorr). This crucial parameter is essential for gaining insights into the electrochemical behavior and overall performance of the electrode. It indicates the resistance that the electrode surface exhibits to current flow when it is slightly perturbed from its equilibrium state, which is vital for evaluating corrosion rates and predicting long-term stability of materials in various environments. The values of Rp have been calculated from Equation 1 [31].

$$RP = \frac{ba\ bc}{2.303(ba+bc)icorr} \quad (1)$$

Where ba and bc represent the anodic and cathodic Tafel slopes, respectively. Rp was calculated as in Table 2, which allows for better design and utilization of electrodes in practical applications. Magnesium and neodymium have relatively close standard electrode potentials, and both are nobler than iron, but more active than boron [32].

Table 2. Corrosion test results for Mg-NdFeB alloy samples

Magnet %	ba(mv)	bc(mv)	$i_{\circ}$ Amps/cm^2	Corrosion rate(mm/a)	$E_{\circ}$(volts)	R_P $\Omega.cm^2 *10^3$
0	43.987	30.531	12.006E-06	0.14084	-0.86285	0.65
3	320.46	159.69	9.1158E-06	0.10694	-0.4151	5.08
4	151.08	225.72	6.4964E-06	0.07621	-0.3934	6.04
10	315.38	169.58	6.1563E-06	0.072221	-0.34951	7.77
20	310.9	156.46	5.0766E-06	0.059554	-0.32842	8.90
30	67.999	127.875	1.532E-06	0.01792	-0.18477	12.58

It is possible to correlate some observed differences in the polarization resistance of the samples with their alloy composition. As shown in Figure 9. Samples with the lowest alloying element concentration demonstrate the lowest resistance against corrosion. On the other hand, samples with the highest nominal alloying element concentration, 30% of NdFeB, demonstrate the lowest corrosion rate of 0.0179 mm/a (millimeters per year). Tafel area as shown in Figure 10. and a corrosive region in the active state, electrode responses to changes in potential are slow until the limit of the Tafel region [33].

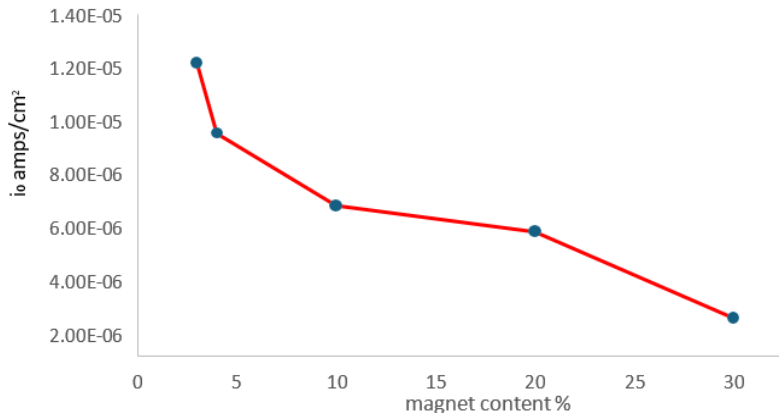

Figure 9. The relation between the current density of Mg-NdFeB and the percentage ratio of the magnet content

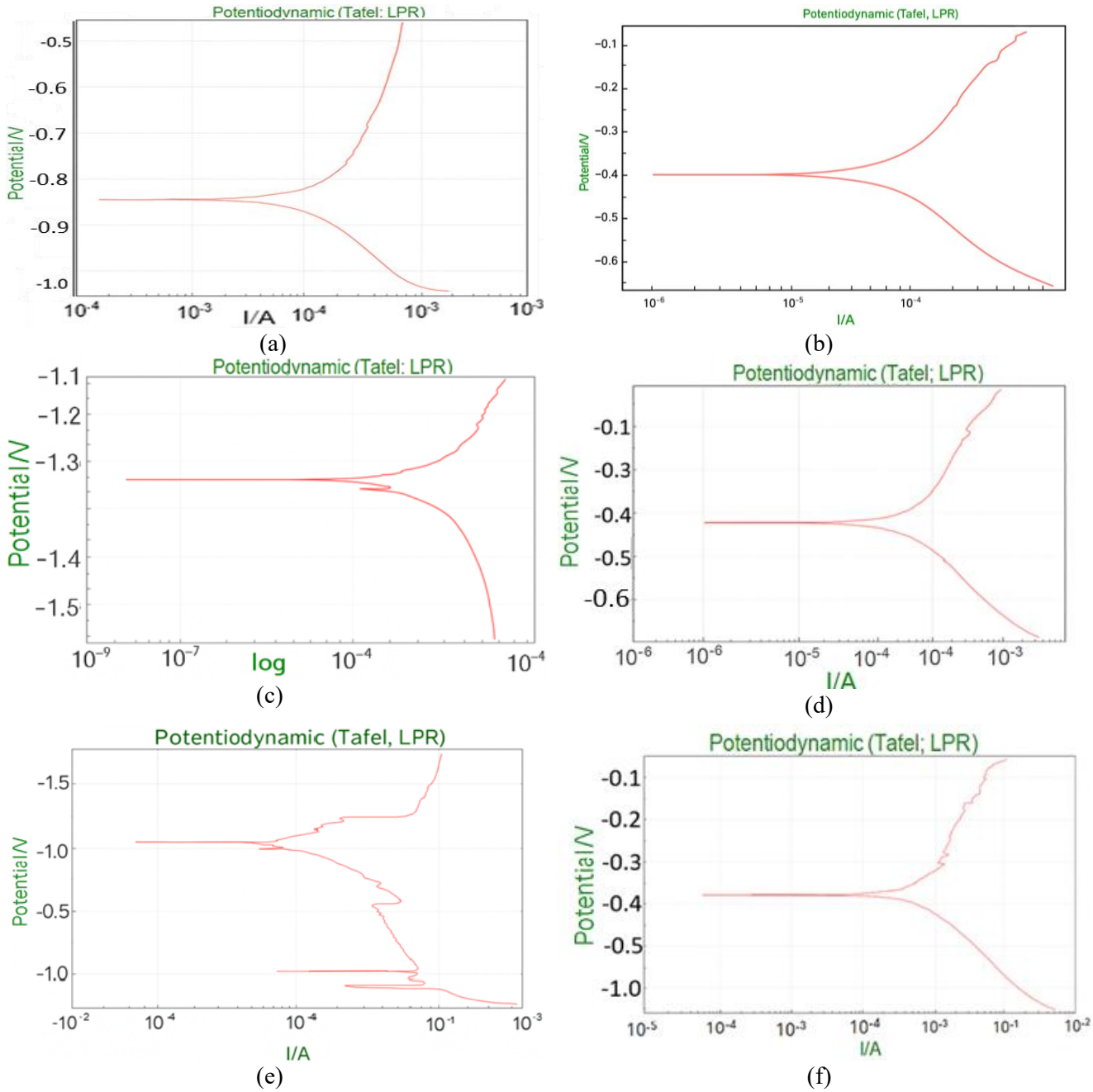

Figure 10. Polarization curve for Mg-Nd-Fe-B alloy with different NdFeB magnet content: (a) pure Mg, (b) 3% (c) 4%, (d) 10%, (e) 20%, (f) 30%

3.5.4. Influence of alloy composition on hardness

The hardness of Mg-Nd-Fe-B alloys, as illustrated in Figure 11, depends on their specific composition and processing conditions. However, the most relevant available data pertains to the Mg-Nd binary alloy, which serves as the foundation for many Mg-Nd-Fe-B systems. For magnesium-neodymium master alloys, the Vickers hardness is typically in the range of 63-67 Hv. These alloys are valued for their precipitation strengthening effect, and the addition of neodymium to magnesium significantly improves hardness and mechanical properties compared to pure magnesium [34].

When iron (Fe) and boron (B) are present, as in Nd-Fe-B or Mg-Nd-Fe-B alloys, the microstructure becomes more complex, often containing hard intermetallic phases such as $Nd_2Fe_{14}B$. This phase is known for its high hardness and is the principal phase in neodymium magnets. Also, the combination of Mg with Nd, Fe, and B, as listed in Table 3, can result in a multiphase microstructure with hard boride and intermetallic phases

dispersed in the Mg matrix (e.g., $Mg_{12}Nd$, FeB, Fe_2B). The result showed that the alloy with a magnetic content 30% had the highest hardness.

Specific Vickers hardness values for the full Mg-Nd-Fe-B system are not widely published in the open literature. However, the presence of $Nd_2Fe_{14}B$ and similar intermetallics would be expected to further increase the overall hardness compared to the Mg-Nd binary alloy alone [35].

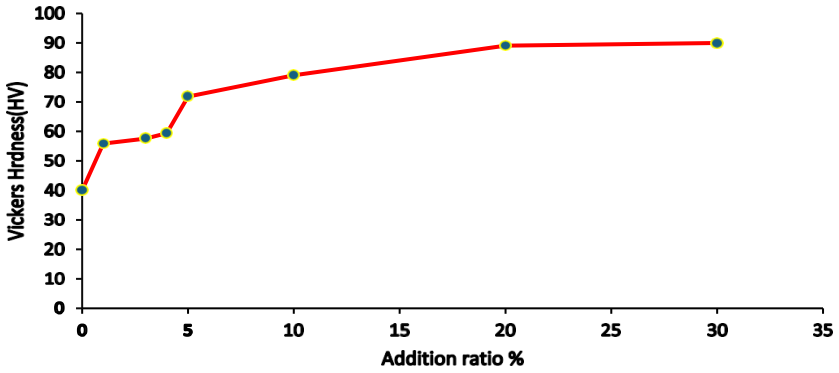

Figure 11. Relation between Vickers hardness of Mg-NdFeB and NdFeB magnet content

Table 2. Alloying effects on hardness for different elements and phases [36]

Element/Phase	Effect on hardness	Notes
Mg	Low base hardness	Ductile, lightweight
Nd	Increases hardness	Precipitation and solid solution hardening
Fe	Increases hardness	Forms hard borides with B
B	Strongly increases hardness	Forms FeB, Fe_2B phases
Nd-Fe-B	Very high hardness (500-650) Hv	Used in permanent magnets
Mg-Nd	Hardness increases with Nd content	Up to an optimal Nd concentration
Fe-B phases	Extremely high microhardness	FeB: up to 27 GPa, Fe_2B: up to 21 GPa

4. Conclusion

The influence of the content of NdFeB on the electrochemical corrosion behavior of Mg-Nd-Fe-B alloys in 3.5% NaCl solution was systematically studied. The Mg-NdFeB showed better resistance against corrosion, especially at 30% content. The presence of the magnet promoted uniform and dense growth of the corrosion product film due to the formation of stable secondary phases, such as $Mg_{12}Nd$ and $Nd_2Fe_{14}B$, which are distributed at grain boundaries and act as microscopic barriers that reduce the progression of localized corrosion and reduce direct interaction between the magnesium matrix and the chloride medium which leading to a decrease in the corrosion rate. Due to the complexity of NdFeB content affecting the corrosion resistance of Mg-Nd-Fe-B alloys, more research needs to be done to explore other proportions of Nd and NdFeB and their effects on the corrosion resistance of Mg-Nd-Fe-B alloys. The presence of iron (Fe) and boron (B), as observed in Nd-Fe-B or Mg-Nd-Fe-B alloys, contributes to a more intricate microstructure, frequently incorporating hard intermetallic phases such as $Nd_2Fe_{14}B$. This specific phase is renowned for its substantial hardness and serves as the primary phase in neodymium magnets. Furthermore, the amalgamation of magnesium (Mg) with neodymium (Nd), iron (Fe), and boron (B) may lead to a multiphase microstructure characterized by the distribution of hard boride and intermetallic phases within the magnesium matrix.

Declaration of competing interest

The authors declare that they have no known financial or non-financial competing interests in any material discussed in this paper.

Funding information

No funding was received from any financial organization to conduct this research.

Author contribution

H.I.A has performed the experimental work, collected and analyzed data, written the first proof, submitted the manuscript, responded to the reviewers' notes, and prepared and submitted the revised manuscript A.A.A has supervised the project, analyzed data, and read and revised the first proof. H.A.A has supervised the project, analyzed data, and read and revised the first proof.

References

[1] B. L. Mordike and T. Ebert, "Magnesium: Properties – applications – potential," *Materials Science and Engineering: A*, vol. 302, no. 1, pp. 37–45, 2001, https://doi.org/10.1016/S0921-5093(00)01351-4

[2] G. Song and A. Atrens, "Understanding magnesium corrosion – a framework for improved alloy performance," *Advanced Engineering Materials*, vol. 5, no. 12, pp. 837–858, 2003, https://doi.org/10.1002/adem.200310405

[3] L. M. Calado, M. J. Carmezim, and M. F. Montemor, "Rare earth based magnesium alloys: a review on WE series," *Frontiers in Materials*, vol. 8, 2021, https://doi.org/10.3389/fmats.2021.804906

[4] X. N. Gu and Y. F. Zheng, "A review on magnesium alloys as biodegradable materials," *Frontiers of Materials Science in China*, vol. 4, no. 2, pp. 111–115, 2010, https://doi.org/10.1007/s11706-010-0024-1

[5] M. Liang, H. Liu, C. Wu, Y. Li, and Z. Guo, "Effects of rare earth neodymium (Nd) and heat treatment on anti-corrosion behaviors of the AZ80 magnesium alloy," *Advanced Composites and Hybrid Materials*, vol. 5, pp. 1460-1476, 2022, https://doi.org/10.1007/s42114-021-00356-4

[6] J. Ni, L. Jin, J. Zeng, J. Li, F. Wang, F. Wang, S. Dong, and J. Dong, "Development of high-strength magnesium alloys with excellent ignition-proof performance based on the oxidation and ignition mechanisms: A review," *Journal of Magnesium and Alloys*, vol. 11, no. 1, pp. 1-14, 2023, https://doi.org/10.1016/j.jma.2022.12.007

[7] X. Wei, L. Ren, Q. Le, Y. Wang, L. Liu, and X. Zhang, "Mg-xNd-Zn-Zr alloys prepared by in-situ reduction: Study of microstructure, corrosion behavior, and mechanical properties," *Materials Today Communications*, vol. 42, p. 111277, 2025, https://doi.org/10.1016/j.mtcomm.2024.111277

[8] O. V. Sukhova, "Formation of structure and properties of boron-rich Fe-BC alloys alloyed with Cr, V, Nb or/and Mo," *Metallophysics and Advanced Technologies*, vol. 43, no. 3, pp. 355-365, 2021, https://doi.org/10.15407/mfint.43.03.0355

[9] L. Xu, X. Liu, K. Sun, R. Fu, and G. Wang, "Corrosion behavior in magnesium-based alloys for biomedical applications," *Materials*, vol. 15, no. 7, p. 2613, 2022, https://doi.org/10.3390/ma15072613

[10] A. A. Luo, "Magnesium casting technology for structural applications," *Journal of Magnesium and Alloys*, vol. 1, no. 1, pp. 2-22, 2013, https://doi.org/10.1016/j.jma.2013.02.002

[11] X. Zeng, "Deformation and recrystallization mechanisms of Mg-Al-Nd and Mg-Zn-Nd alloys," Theses, 2021, https://doi.org/10.14279/depositonce-12420

[12] T. Yamada, J. Yin, and K. Tanaka, "Hydrogen storage properties and phase structures of Mg-rich Mg-Pd, Mg-Nd and Mg-Pd-Nd alloys," *Materials Transactions*, vol. 42, no. 11, pp. 2415-2421, 2001, https://doi.org/10.2320/matertrans.42.2415

[13] Z. Gui, Y. Huang, X. Li, and M. Zhao, "Corrosion behavior of as-cast and solution-treated Mg-xGd-1.5Nd-0.5Zn-0.5Zr alloys," *Corrosion Science*, vol. 176, no. 3, p. 109004, 2020, https://doi.org/10.1016/j.corsci.2020.109004

[14] D. Liu, D. Yang, X. Li, and S. Hu, "Mechanical properties, corrosion resistance and biocompatibilities of degradable Mg-RE alloys: A review," *Journal of Materials Research and Technology*, vol. 8, no. 1, pp. 1538-1549, 2019, https://doi.org/10.1016/j.jmrt.2018.08.003

[15] N. Kalkoul, N. Boussouf, and S. Mahjoub, "Addition effects of MgO on structure and physical properties in Bi-2212 ceramics," *Annales de Chimie-Science des Matériaux*, vol. 46, no. 6, pp. 295-299, 2022, https://doi.org/10.18280/ACSM.460602

[16] H. Dong, K. He, X. Meng, H. Xu, G. Ming, and Y. Du, "Influence of laser powder bed fusion scanning strategies on the magnetic and mechanical properties of NdFeB," *Journal of Alloys and Compounds*, vol. 1020, p. 179384, 2025, https://doi.org/10.1016/j.jallcom.2025.179384

[17] S. Luo, X. Gao, M. Yang, S. Zhong, and X. Yu, "Effect of texture intensity on grain boundary diffusion in sintered NdFeB magnets," *Journal of Materials Research and Technology*, vol. 35, pp. 4734-4744, 2025, https://doi.org/10.1016/j.jmrt.2025.02.117

[18] J. Huang, M. Huang, F. Wang, and Z. Wang, "Microstructure optimization and coercivity enhancement of sintered NdFeB magnet by grain boundary diffusion of multicomponent Tb60Pr10Cu10Al10Zn10 films," *Materials*, vol. 16, no. 8, p. 3131, 2023, https://doi.org/10.3390/ma16083131

[19] S. Abu al Noun, A. Faeza Ali Sameer, and N. Izat Abdulatif, "Separation of Aluminum Chloride from White Kaolinite by Slime Leaching Process," *Engineering & Technology Journal*, vol. 32, no. 24, pp. 12-0758, 2014, https://doi.org/10.30684/etj.32.7A8

[20] R. A. Majed, M. Mahdi, and H. A. AL-Kaisy, "Corrosion behavior of Al-Cu-Mg alloy by addition of SiO2 particles in seawater," *Engineering & Technology Journal*, vol. 32, pp. 118-131, 2014, https://doi.org/10.30684/etj.32.1A.10

[21] S. R. Areef, "Effect of (Zn & Mg) on corrosion behavior of shape memory alloys," *Engineering & Technology Journal*, vol. 28, pp. 5651-5659, 2010, https://doi.org/10.30684/etj.28.18.3

[22] B. Yao, N. Kang, X. Li, D. Li, and M. E. L. Mansori, "Toward understanding the microstructure characteristics, phase selection and magnetic properties of laser additive manufactured Nd-Fe-B permanent magnets," *Journal of Extreme Manufacturing*, vol. 6, p. 015002, 2024, https://doi.org/10.1088/2631-7990/ad0472

[23] D. Escalera-López, S. Czioska, J. Geppert, et al., "Phase-and surface composition-dependent electrochemical stability of Ir-Ru nanoparticles during oxygen evolution reaction," *ACS Catalysis*, vol. 11, pp. 9300-9316, 2021, https://doi.org/10.1021/acscatal.1c01682

[24] P. Liu, G. Zhang, H. Xu, and S. Cheng, "Synergistic dielectric–magnetic enhancement via phase-evolution engineering and dynamic magnetic resonance," *Advanced Functional Materials*, vol. 33, no. 13, p. 2211298, 2023, https://doi.org/10.1002/adfm.202211298

[25] L. Wang and X. Xu, "Facile synthesis of Nd2Fe14B hard magnetic particles with microwave-assisted hydrothermal method," *Molecules*, vol. 28, no. 23, p. 7918, 2023, https://doi.org/10.3390/molecules28237918

[26] Q. Huang, Q. Lin, Y. Xu, and Y. Cao, "Predicting potential hard materials in NbB ternary boride: First-principle calculations," *Journal of Refractory Metals and Hard Materials*, vol. 126, p. 106927, 2025, https://doi.org/10.1016/j.ijrmhm.2024.106927

[27] R. Bender, D. Féron, D. Mills, and S. Ritter, "Corrosion challenges towards a sustainable society," *Materials and Corrosion*, vol. 73, no. 17, pp. 30-1751, 2022, https://doi.org/10.1002/maco.202213140

[28] R. Shen, S. Xu, C. Wang, E. Yang, X. Liu, and S. Fu, "Concurrent improvements in coercivity and corrosion resistance for Nd6Fe13Ga-reconstructed Nd–Fe–B sintered magnets," *Journal of Materials Chemistry C*, vol. 13, no. 1, 2025, https://doi.org/10.1039/D4TC04062G

[29] Z. Li, M. Zhu, X. Song, Z. Deng, D. Zhang, and X. Wu, "Low thermal expansion and corrosion resistance characteristics of high-coercivity Nd-Fe-B magnets through Tb Mg diffusion," *Journal of Materials*, vol. 245, pp. 175-181, 2025, https://doi.org/10.1016/j.jmst.2025.04.033

[30] Y. Gao, G. Bai, H. Hou, and Y. Zhao, "First-principle investigation of the influence of rare earth element doping on the corrosion characteristics of Mg(0001) surface," *Physica B: Condensed Matter*, vol. 710, p. 417198, 2025, https://doi.org/10.1016/j.physb.2025.417198

[31] R. Aslam, "Potentiodynamic polarization methods for corrosion measurement," in *Electrochemical and Analytical Techniques for Sustainable Corrosion Monitoring*, pp. 25-37, 2023, https://doi.org/10.1016/B978-0-443-15783-7.00003-7

[32] C. Nyby, X. Guo, J. E. Saal, S. C. Chien, A. Y. Gerard, and H. Ke, "Electrochemical metrics for corrosion resistant alloys," *Scientific Data*, vol. 8, no. 1, 2021, https://doi.org/10.1038/s41597-021-00840-y

[33] M. Li, H. Henein, C. Zhou, and J. Liu, "Towards high-entropy alloys with high-temperature corrosion resistance and structural stability," *Journal of Materials Science & Technology*, vol. 174, pp. 133-144, 2024, https://doi.org/10.1016/j.jmst.2023.07.035

[34] T. Tamam, M. Z. Touhami, and M. Zahzouh, "Microstructural, mechanical and corrosion characterizations of borided cast irons formed by a recycled boriding agent," *Journal of Materials*, vol. 33, pp. 194-212, 2024, https://doi.org/10.1007/s11665-023-07978-3

[35] B. Białobrzeska, "Effect of alloying additives and micro additives on hardenability increase caused by action of boron," *Metals*, vol. 11, no. 4, p. 589, 2021, https://doi.org/10.3390/met11040589

[36] Z. Liu, J. He, Q. Zhou, Y. Huang, and Q. Jiang, "Development of non-rare earth grain boundary modification techniques for Nd-Fe-B permanent magnets," *Journal of Materials Science and Technology*, vol. 98, pp. 51-61, 2022, https://doi.org/10.1016/j.jmst.2021.05.012